Modelling simultaneous precipitation reactions in austenitic stainless steels

T. Sourmail*, H.K.D.H. Bhadeshia

Department of Materials Science and Metallurgy, University of Cambridge, Pembroke Street, Cambridge CB2 3QZ, UK

Received 3 June 2003

Abstract

A physical model has been developed for simultaneous precipitation reactions in austenitic stainless steels, taking into account interactions between phases. Comparisons against experimental results show satisfying agreement, with the model successfully predicting the existence of transient phases that are often observed, but not predicted in equilibrium calculations. An analysis of σ-phase kinetics, especially the effect of grain size, supports the hypothesis that the formation of this phase depends more on the availability of high energy nucleation sites than on the driving force for its formation. The study underlines a lack of thermodynamic data for important phases in creep-resistant austenitic stainless steels.

© 2003 Elsevier Ltd. All rights reserved.

1. Introduction

Precipitation phenomena in creep-resistant austenitic stainless steels are numerous and complex, with a large number of possible phases forming during long term exposure to high temperature [1]. The occurrence of these different precipitates are interdependent and sensitive to small composition changes [1, 2]. Any attempt to model the decomposition of austenite into several phases should therefore take into account the competition for solute and nucleation sites and space. Recent works by Robson and Bhadeshia [3], or Fujita and Bhadeshia [4] have demonstrated the possibility to model interaction between various precipitation reactions in steels. This work is concerned with the development and improvement of a similar model for austenitic stainless steels.

2. Model

2.1. Growth rate in binary systems

Precipitates have been approximated to be of spherical shape throughout. The diffusion-controlled growth rate of a spherical particle in a binary system is a well-studied problem [5], for which the solution can be written:

$$\psi = \frac{S\sqrt{D}}{2\sqrt{t}} \tag{1}$$

where ψ is the velocity of the interface, D the diffusivity of solute in the matrix, and S is the solution of:

$$S^3 = 2 * \Omega * \frac{\exp(-\frac{S^2}{4})}{\Phi(S)} \tag{2}$$

with $\Omega = (\overline{c} - c^{\gamma\theta})/(c^{\theta\gamma} - c^{\gamma\theta})$ where $c^{\theta\gamma}$ refers to the concentration of the phase θ in equilibrium with γ, and $\overline{c}$ is the bulk composition of the binary system (Fig. 1). $\Phi(S)$ is given by:

$$\Phi(S) = \int_S^\infty u^{-2} \exp\left(-\frac{S^2}{4}\right) du. \tag{3}$$

For small supersaturations ($\Omega \to 0$) this can be approximated by $S \approx \sqrt{2\Omega}$ while for large supersaturations ($\Omega \to 1$), $S \approx \sqrt{6/(1-\Omega)}$; further details can be found in [6].

2.2. Growth rate in a multicomponent alloy

In a multicomponent alloy, assuming local equilibrium at the interface, the interface composition is given by the tie-line satisfying the set of equations [7]:

---

* Corresponding author.
  E-mail address: ts228@cus.cam.ac.uk (T. Sourmail).
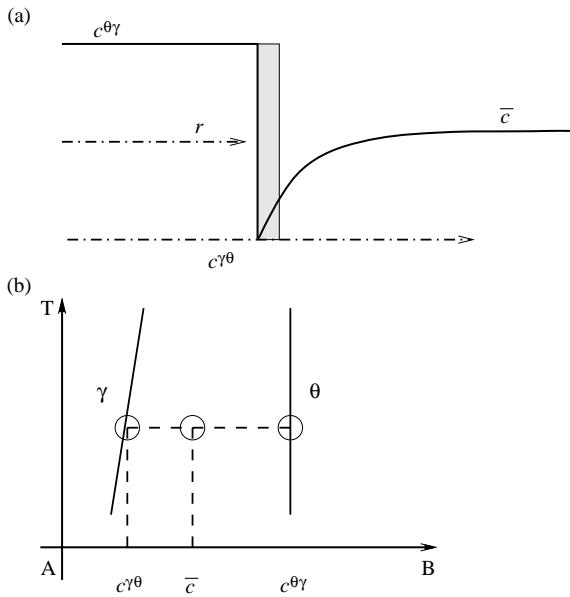
Fig. 1. (a) The concentration profile of the element i as a function of the distance from the interface matrix/precipitate. (b) Relationship with the phase diagram. r is the radial coordinate, the value of which is r_i at the interface.

Fig. 2. The flux-balance tie-line going through M can be significantly different from the mass-balance one, that passes through P the bulk composition.

$$J_i = \psi(c_i^{\theta\gamma} - c_i^{\gamma\theta}) \qquad i = 1, \ldots, n-1 \tag{4}$$

where n is the number of elements in the system, the index i refers to the element i, with $c_i^{\gamma\theta}$ the concentration in γ in equilibrium with θ.

When two solutes have significantly different diffusivities, the particular tie-line which allows the set of Eq. (4) to be satisfied, i.e. the flux-balance tie-line, will in general be different from that passing through $\overline{c_i}$, as illustrated in Fig. 2 for a ternary system.

2.3. Nucleation rate

Classical theory for nucleation suggests that the nucleation rate I is given by:

$$I_\theta = N \exp\left(-\frac{G_\theta^*}{RT}\right) \nu \exp\left(-\frac{G_t^*}{RT}\right) \tag{5}$$

where G_θ^* is the activation energy for the nucleation of θ and G_t^* the activation energy for the transfer of atoms across the γ/θ interface; N is the number density of nucleation sites and ν is an attempt frequency taken as being kT/h. For a spherical precipitate θ, the activation energy for nucleation is given by [5]:

$$G_\theta^* = \frac{16\pi}{3} \frac{\sigma_{\gamma\theta}^3 V_m^{\theta 2}}{\Delta G_{m,\theta}^2} \tag{6}$$

where V_m^θ is the molar volume of θ, $\sigma_{\gamma\theta}$ the energy per unit area of the interface γ/θ, $\Delta G_{m,\theta}$ the driving force for the precipitation of θ, per mole of components in θ.

2.4. Overall transformation kinetics

Calculations were carried out in discrete time steps to evaluate the volume fractions of the different precipitates expected to form. At the end of each time step, the average matrix concentration was updated according to:

$$d\overline{c_i} = \sum_\theta \frac{(\overline{c_i} - c_i^{\theta\gamma})dV_{f,\theta} - \overline{c_i}}{V_{f,\gamma}} \tag{7}$$

where $d\overline{c_i}$ is the change of matrix composition, $dV_{f,\theta}$ the change of volume fraction for the precipitate θ. The computer program for the model was interfaced with MT-DATA [8], in order to re-evaluate the driving forces and local equilibria after each modification of the matrix composition. Nucleation growth rates are then re-calculated and the process is repeated in order to follow the evolution of the microstructure.

In the classical Avrami theory, or in its adaptation to simultaneous reactions [3], the increase in volume fraction is corrected to account for the presence of transformed regions. This correction was neglected throughout, a reasonable approximation given the small volume fractions involved.

Table 1
The diffusion coefficient of Cr in AISI 316 at 750 °C as calculated and found in different studies

Material	Calculated (m² s⁻¹)	Literature (m² s⁻¹)
AISI 316 [12]	8.9×10^{-19}	6.2×10^{-19}
16Cr–14Ni [13]	5.54×10^{-19}	5.50×10^{-19}

2.5. Diffusion coefficients and other parameters

A number of recent studies have focussed on providing diffusion data in a framework similar to what CALPHAD is to phase calculations. Data published by Jönsson [9], Ågren [10] and Andersson and Ågren [11] have been used to calculate the diffusion coefficient of carbon and chromium as a function of composition. This calculation is performed within the overall model using the initial composition of the matrix. Table 1 provides examples of calculated diffusion coefficients together with values found in the literature. Jönsson [9] made extended comparison with measurements of the carbon diffusivity and it was verified that his results were satisfyingly reproduced.

Data were less readily available for Nb, Ti and Mo for these steels, and these coefficients, when required in calculations were set to be equal to that of chromium. Similarly, in all cases, the activation energy for transfer across the nucleus interface G_t^* was taken to be about the activation energy for chromium diffusion, 250 kJ mol^{-1}.

3. Implementation and results

3.1. Identifying the flux-balance tie-line

Of all precipitate phases likely to form in austenitic stainless steels (MX, $M_{23}C_6$, σ, etc., see [1]), the difference between flux and mass-balance tie-lines was found to be significant only for $M_{23}C_6$. The small predicted difference for MX type precipitates (NbC, TiC, NbN, TiN) is because these phases are modelled in the thermodynamic databases as pure substances, whose compositions are fixed by stoichiometry. However, experimental results [14, 15] have shown that such precipitates start growing with a composition different from equilibrium, the difference being attributed to the shift in the flux-balance tie-line as precipitation progresses [1, 14]. Because of the assumed stoichiometry, it is not possible in the present work to properly model MX precipitates. For intermetallics (σ, Laves, etc.), the diffusivities of the different elements involved are similar therefore leading to only a small difference between the mass and flux-balance tie-line.

For the case of $M_{23}C_6$, the following approximations were made when evaluating the local equilibrium at the transformation front. Because the diffusion coefficient of carbon is larger than that of the substitutional elements, it was assumed that carbon achieves a uniform activity instantaneously. Once the tie-line consistent with carbon isoactivity was identified, the interface velocity was calculated on the basis of the corresponding chromium flux:

$$J_{Cr} = -D_{Cr}\nabla c_{Cr} - D_{CrC}\nabla c_C \approx -D_{Cr}\nabla c_{Cr} \qquad (8)$$

where the cross-diffusion D_{CrC} term can be reasonably neglected.
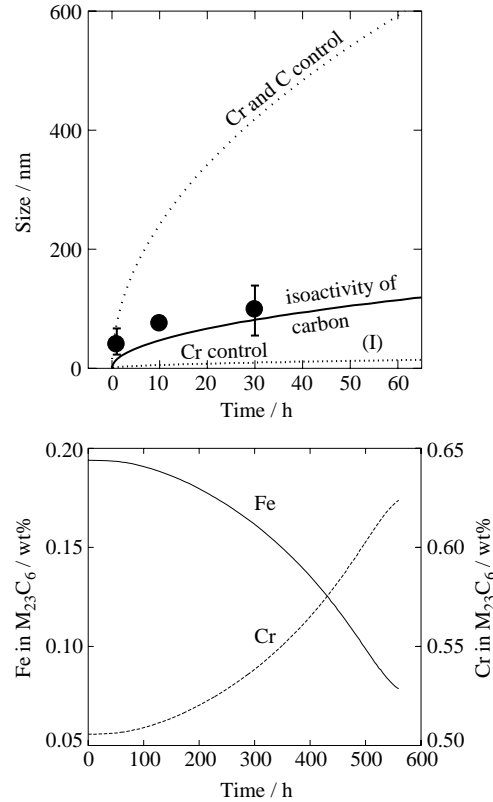
Fig. 3. Comparison between measured and calculated size for $M_{23}C_6$ in AISI 316 aged at 650 °C, using different models, and example of evolution of the composition of $M_{23}C_6$ with time.

As illustrated in Fig. 3, the calculated growth rate of $M_{23}C_6$ compares well with data obtained by Záhumenský et al. [12] for a type 316 steel at 650 °C. Alternative models have used the Cr gradient as defined by the mass-balance tie-line [3, 16], labelled Cr-control in Fig. 3, or the zero carbon-gradient tie-line [4], labelled Cr–C control in Fig. 3. These methods have been shown to under or over estimate the actual growth rate respectively.

Table 2
The Cr/Fe ratio in $M_{23}C_6$ in different cases, for the AISI 304 steel studied by Boeuf et al. The last method clearly gives satisfying agreement with experimental results

	Cr/Fe ratio
Equilibrium	12
Boeuf et al. at $t = 0$	**2.1**
Carbon zero-gradient	0.72
Carbon isoactivity	**2.2**

Further validation for this method is obtained when comparing measured and predicted Cr/Fe ratios in $M_{23}C_6$: it has frequently been reported [15, 17, 18] that the ratio Cr/Fe is significantly lower at the early stages of precipitation than it is at equilibrium, and gradually increases with ageing time. Such behaviour is correctly predicted by the model (Fig. 3).
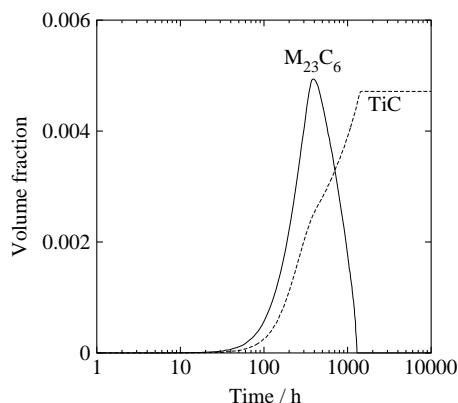
Fig. 4. The calculated volume fraction of $M_{23}C_6$ and TiC as a function of time in an AISI 321 steel, during ageing at $750\,^\circ$C. $M_{23}C_6$ is expected as a transient phase only. The volume fraction of TiC does not include the amount left undissolved after solution treatment.

Table 2 compares the predicted initial composition of $M_{23}C_6$ in AISI 304 to the measured values given by Boeuf et al. [17].

3.2. Competition for solute

As mentioned earlier, the interactions between precipitation reactions are essential in the understanding of the sequences of reactions occurring in austenitic stainless steels. A typical example is the case of stabilised austenitic stainless steels, where addition of strong carbo-nitride formers such as Nb or Ti are made to suppress the formation of $M_{23}C_6$. The latter is however reported to exist as a transient phase (Fig. 4). The AISI 321 steel (17.1Cr, 12.6Ni, 1.5Mn, 0.5Si, 0.49Ti, 0.11C wt%) as studied by Thorvaldsson [19] is a good example of the importance of interactions in precipitation sequences.

It should be noted that the behaviour and final amount of phases are dictated by the underlying thermodynamic models. In this case, TiC is predicted to be the stable phase. Discrepancies have been reported [1] on the behaviour of Ti stabilised steels.

In general, there is little quantitative information regarding precipitation in austenitic stainless steels. Furthermore, results obtained by different methods differ significantly. For example, the work utilised in the previous section, from Thorvaldsson and Dunlop [19], indicates that the maximum volume fraction of MC type carbides (mainly TiC) is reached after about 1000 h, on the basis of TEM investigations. On the other hand, Thorvaldsson et al. [15], in a different publication on a similar steel, for identical conditions, report the maximum volume fraction of MC type carbides (mixed (Ti, Nb)C) to be reached after 3–8 h, on the basis of resistance measurements. There are no comments from the authors as to the largely different kinetics of precipitation.

This makes it difficult to estimate the adjustable parameters N and $\sigma_{\gamma\theta}$ for these phases. However, the time scale for the formation of such carbides and nitrides remains
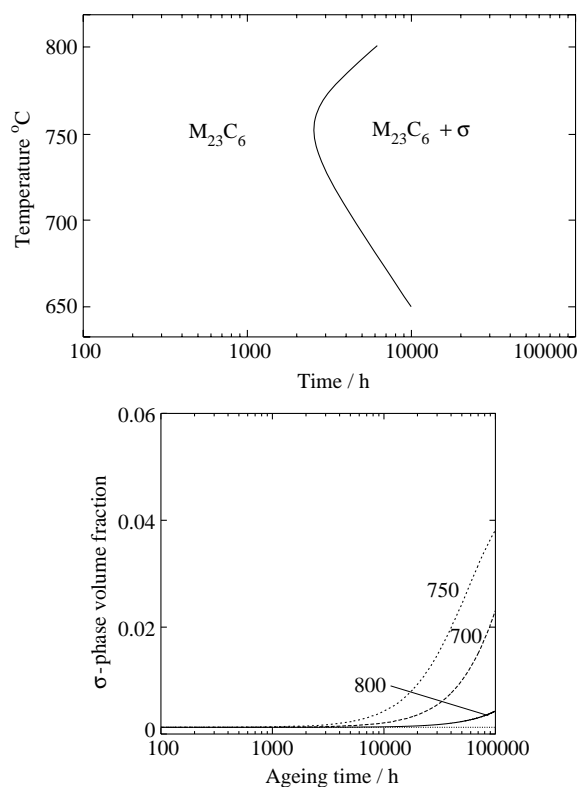
Fig. 5. TTP diagram for the formation of σ in an AISI 304 steel of composition: 18.7Cr, 9.0Ni, 1.73Mn, 0.6Si, 0.05C wt%. Predictions (bottom), with indication of the temperature in $^\circ$C, are compared to the TTP diagram obtained by Minami et al. [20] (top). The nose of the TTP curve is in both cases obtained at $750\,^\circ$C.

small in comparison with the typical lifetime in creep, and therefore the error introduced in the precipitation sequence is of little consequence.

3.3. The formation of σ-phase in the AISI 300 series

3.3.1. Identifying the nucleation parameters for AISI 304

The case of σ-phase, which incidentally is believed to be more relevant to long term creep properties than the various carbides, is better defined. Minami et al. [20] provide data on the microstructural evolution of the main AISI 300 series steels, which have been used to refine the parameters N_σ and $\sigma_{\gamma\sigma}$ (respectively the number density of nucleation sites for σ-phase and the interfacial energy between σ-phase and austenite).

With $N_\sigma = 2.3 \times 10^{12}$ m^{-3} and $\sigma_{\gamma\sigma} = 0.252$ J m^{-2}, satisfying agreement was obtained between the predictions and both the time–temperature–precipitation (TTP) diagram and the quantitative measurements provided by these authors (Figs. 5 and 6).

The disagreement at high temperatures is essentially due to thermodynamic data on which the calculations rely: the NPL PLUS database (based on SGTE SSOL) predicts an equilibrium amount of σ-phase (1.7%) which is not consistent with the observations made by Minami et al. [20].
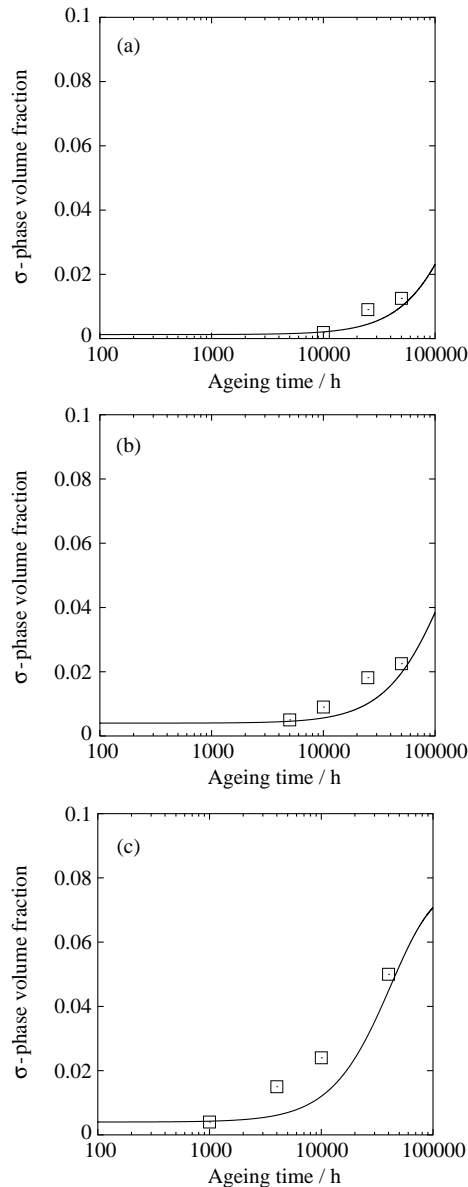
Fig. 6. The rate of formation of σ-phase at 700 °C in (a) AISI 304, (b) AISI 316 and (c) AISI 347. For 316 and 347 (1) the calculated line is obtained with the prefactor fitted with the data for 304 [20], corrected for the grain size difference.

Furthermore, this fitting can only be semi-quantitative, as there remains the problem of the detection limit, which may not scale with the volume fraction: at high temperature, few precipitates of large size are expected, while at low temperature, one expects smaller but more numerous precipitates. This means that, unless an exact determination of the volume fraction is carried out, σ-phase might be detected at lower volume fraction at high temperatures.

3.3.2. Observed and predicted trends in the AISI 300 series

Fig. 6 shows the evolution of the volume fraction of σ-phase as a function of ageing time at 700 °C, in different steels of the AISI 300 series.

Initially, the nucleation parameters obtained for AISI 304 were used to predict the formation of σ-phase in 316 (304 with Mo) and 347 (Nb-stabilised). The results were opposite to the observed trends, with the formation of σ predicted to be slowest in 347, where it is observed to be the fastest. This problem is directly related to the predicted driving forces in the different steels, shown in Table 3.

However, examination of the different micrographies published in [20] revealed considerable difference in grain sizes between 304 and 347. The mean linear intercept was estimated to be 3.7 times smaller in the latter steel. The nucleation site density was therefore corrected so as to account for the smaller grain size: the model essentially considers grain boundary nucleation, implying that the number density should be 3.7^2 greater in 347 than in 304. Once this correction is made, better agreement is obtained as 347 is correctly predicted to occur faster in 347 than in 304, despite the lower driving force. Calculations with the corrected nucleation parameters are shown in Fig. 6.

The predicted increase is generally slightly steeper than that measured. It was verified however, that saturation of the nucleation sites was reached in the very early stages of the precipitation, which corresponds to the least steep curve for a given growth rate. The explanation for the discrepancy was therefore expected to be found in the simple growth model adopted.

It must be emphasised at this point that very few of the parameters in this model are user-selected; for example, diffusion coefficients, interface compositions and driving forces are indirectly provided by thermodynamic databases, there is therefore little lattitude to modify the calculated growth rate for a given phase using the 'natural' parameters such as diffusion coefficient, supersaturation etc.

By artificially multiplying the interface velocity for σ-phase by a factor varying between 0.2 and 1.5, the effect on the steepness of the growth curves could be investigated. It was found that, once the nucleation site density modified to obtain curves located at the same times, the gradient of the volume fraction vs. time curves was not significantly changed. Furthermore, the final particle sizes obtained for σ-phase were in best agreement with typical sizes observed in [20] when the growth rate was left unchanged, with predicted sizes of 3.8 μm after 50 000 h at 700 °C, compared to an observed size of 4.2 μm in the AISI 347 studied in [20]. It is therefore concluded that the difference is not the result of the simple growth model adopted, but is most likely the result of the mean-field approximation, as only an enhanced soft-impingement could further decrease the steepness of the volume fraction vs. time curves. Further work is required in order to improve on this approximation.

Barcik [21] proposed that σ phase formation is most strongly affected by grain size, that is, by nucleation site density. Minami et al. [20] have opposed this viewpoint, and proposed that the driving force is a predominant factor in the rate of σ-phase formation. However, the present study, on the basis of their own data, indicates that, although the

Table 3
The composition of different steels studied by Minami et al. [20], after precipitation of all carbides, calculated with MT-DATA [8], and the driving force for the formation of σ-phase from the austenite of this composition, expressed in joules per mole of components. All calculations are for 700 °C. All alloys have an initial carbon content of 0.05 wt%, the initial substitutional content of 304 and 316 is hardly changed, while in 347 the initial Nb content is of 0.59 wt%, reduced by precipitation of NbC

Element wt%	Cr	Ni	Mn	Si	Ti	Nb	C	ΔG_m (J mol^{-1})
AISI 304	18.20	9.07	1.73	0.60			2.15×10^{-3}	−209.7
AISI 347	17.68	10.45	1.65	0.59		0.48	4×10^{-5}	−169.7
AISI 316 (2.3 Mo)	16.09	12.01	1.83	0.64			5.4×10^{-4}	−288.4
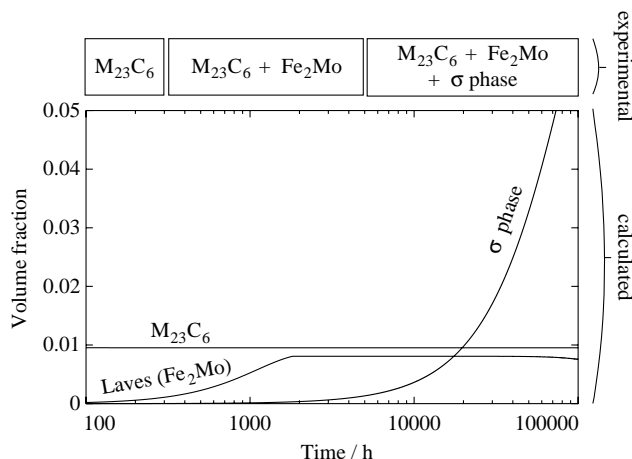
Fig. 7. The evolution of the volume fraction of different phases in an AISI 316 steel at 700 °C, and on the upper part, the phases observed experimentally by Minami et al. [20].

driving force might have an effect, it is expected to be of small influence compared to the grain size, or any other parameter which could result in an increase in nucleation site density. In fact, use of the driving force alone leads to predictions of trends opposite to the observed ones.

Calculations indicate, in general, that σ-phase is considerably more difficult to nucleate than most carbide phases, and therefore confined to relatively high-energy defects. This suggests that the method recently used to control sensitisation [22], by which the average grain boundary energy is reduced by a carefully designed thermo-mechanical treatment, may also lead to suppression, or significant delay, of σ-phase formation.

The validity of these conclusions is obviously dependent on that of the predicted driving forces, that is, ultimately, on the thermodynamic database used in this study (NPL plus, based on SGTE SSOL), and on the hypothesis that the interfacial energy $\sigma_{\gamma\sigma}$ does not vary significantly between the three grades. This seems a reasonable assumption given their similar compositions.

3.4. Example of full precipitation sequence

Fig. 7 shows the complete precipitation sequence for an AISI 316 steel, at 700 °C, which is in good agreement with

the work of Minami et al. [20]. However, at 750 °C, χ phase is found experimentally, but is not predicted to form by the model. This is because, according to MT-DATA, the driving force for its formation is zero throughout the precipitation sequence.

It is important to note that a simple equilibrium calculation will not predict the presence of Laves phase (Fe_2Mo), which only exists as a transient phase, and dissolves as σ-phase precipitation progresses. Although there is no driving force for the formation of Laves phase once σ-phase is formed, this is not the case if the supersaturated matrix composition is considered. In a similar way, there is a driving force for precipitation of $M_{23}C_6$ from the initial supersaturated matrix, in the example illustrated in Fig. 4, however TiC is ultimately the only stable carbide.

4. Conclusions

A physically-based model to predict precipitation sequences has been presented that accounts for interactions between the different kinds of phases forming in austenitic stainless steels. The underlying growth model was shown to give satisfying quantitative agreement when required thermodynamic data were available. The overall kinetics are in satisfying agreement with the published observations, particularly in regard of the relative simplicity of the model. However, this success is necessarily limited to phases for which thermodynamic data are available.

This is unfortunately not the case for a number of phases observed in austenitic stainless steels: in Nb rich steels (AISI 347) in which Fe_2Nb and Fe_3Nb_3C are expected to form when Nb is in excess [1]. Although the formation of the former is correctly predicted, its dissolution for the latter cannot be accounted for, since there are no thermodynamic data for Fe_3Nb_3C. Phases such as Cr_3Ni_2SiX or Z-phase are not represented in the SGTE database, therefore making difficult any meaningful prediction on nitrogen bearing steels.

It was shown that the composition change of $M_{23}C_6$ can be correctly predicted which suggests it could be used as an indicator of the progress of the precipitation. The present model also supports the suggestion that σ-phase formation depends above all on the number of high-energy nucleation sites, the driving force being of lesser importance.

The code for the corresponding software is freely available on http://www.msm.cam.ac.uk/map/, together with the data used for the predictions shown in the present publication.

Acknowledgements

References

[1] T. Sourmail, Mater. Sci. Technol. 17 (2001) 1–14.
[2] A.F. Padilha, P.R. Rios, I.S.I.J. International 42 (2002) 325–337.
[3] J.D. Robson, H.K.D.H. Bhadeshia, Mater. Sci. Technol. 13 (1997) 631–639.
[4] N. Fujita, H.K.D.H. Bhadeshia, Mater. Sci. Technol. 15 (1999) 627–634.
[5] J.W. Christian, Theory of Transformation in Metals and Alloys, Pergamon Press, Oxford, 1975.
[6] T. Sourmail, Ph.D. Thesis, Department of Materials Science and Metallurgy, University of Cambridge, 2002. Available from http://www.msm.cam.ac.uk/phase-trans.
[7] D.E. Coates, Metall. Trans. 3 (1972) 1203–1212.
[8] MT-DATA, National Physical Laboratory, Teddington, UK (1989).
[9] B. Jönsson, Z. Metallkd. 85 (1994) 502–509.
[10] J. Ågren, I.S.I.J. International 32 (1992) 291–296.
[11] J.-O. Andersson, J. Ågren, J. Appl. Phys. 72 (4) (1992) 1350–1355.
[12] P. Záhumenský, P. Ševc, J. Janovec, Kovo. Mater. 37 (1999) 108–119.
[13] W. Assassa, P. Guiraldenq, Met. Corros. Ind. 621 (1977) 170–175.
[14] H.O. Andrén, A. Henjered, H. Norden, J. Mater. Sci. 15 (1980) 2365–2368.
[15] T. Thorvaldsson, H. Rubinsztein-Dunlop, H.-O. Andrén, G.L. Dunlop, Quantitative Microanalysis with High Spatial Resolution, The Metals Society, 1981, pp. 250–254.
[16] R.G. Faulkner, H. Jiang, Mater. Sci. Technol. 9 (1993) 665–671.
[17] A. Boeuf, R. Coppola, F. Zamboni, J.P. Morlevat, F. Rustichelli, D. Wenger, J. Mater. Sci. 16 (1981) 1975–1979.
[18] J. Barcik, Mater. Sci. Technol. 4 (1988) 5–15.
[19] T. Thorvaldsson, G.L. Dunlop, Metal Sci. 16 (1981) 513–518.
[20] Y. Minami, H. Kimura, Y. Ihara, Mater. Sci. Technol. 2 (1986) 795–806.
[21] J. Barcik, Metall. Trans. A 14 (1983) 635–641.
[22] M. Shimada, H. Kokawa, Z.J. Wang, Y.S. Sato, I. Karibe, Acta Mat. 50 (2002) 2331–2341.